Coherent effects in spectrally resolved pump-probe differential reflectivity measurements at exciton resonance in GaAs quantum wells

Bipul Pal* and A. S. Vengurlekar
Tata Institute of Fundamental Research, Mumbai 400005, India

(Received 7 October 2002; revised manuscript received 5 May 2003; published 10 September 2003)

We perform femtosecond spectrally resolved pump-probe differential reflectivity measurements on excitons in GaAs quantum wells in both coherent and incoherent regimes. The spectral signal is nonzero and oscillatory at $-ve$ delay up to a few ps indicating persistent coherence between excitonic polarization induced by the probe pulse and the delayed pump pulse. The signal for small $+ve$ and $-ve$ delay (τ) shows modulation caused by quantum beats due to coexcitation of heavy and light hole excitons. The rise of the signal with τ for $\tau<0$ is rather nonexponential and is sensitive to detuning of the detection energy with respect to the exciton energy. The signal decay with τ for small $+ve$ τ shows dependence on pump-probe relative polarization. The excitonic reflectivity shows a large reduction caused by excitonic absorption saturation for both $+ve$ and $-ve$ τ when the pump pulse intensity is increased to large values. To compare the experimental results with theory, we obtain an expression for the PPDR signal in terms of the third order excitonic polarization. This has an additional term not considered earlier to describe pump-probe experiments. The calculations are performed using optical Bloch equations, modified to incorporate exciton inhomogeneous broadening, quantum beats, and many body effects such as local field, excitation induced energy shift, and dephasing. These effects are found essential in explaining the observed PPDR spectral data. The delay dependence of the signal near the exciton energy is mainly controlled by inhomogeneous broadening for $-ve$ τ. The signal decay for large $+ve$ τ has an exponential behavior determined by the lifetime of incoherent excitons. Experiments for collinear polarization reveal an additional exponential component for small $+ve$ delay. Theoretically, this is found to be related to exciton dephasing and is present only when many body effects are included.

DOI: 10.1103/PhysRevB.68.125308 PACS number(s): 71.35.−y, 42.50.Md, 78.47.+p, 78.67.De

I. INTRODUCTION

Pump-probe differential reflectivity (PPDR) measurements have been extensively performed in the past on free carriers excited in semiconductors using ultrashort laser pulses to study hot carrier thermalization and relaxation,[1] and to estimate carrier recombination lifetime[2] for materials suitable for efficient THz radiation generation and for ultrafast photoconductive applications. In comparison, fewer and less detailed studies of modulated reflectivity are available in the case of resonant excitation at the exciton energy, relevant in some applications such as quantum well (QW) saturable absorber mirrors.[3] The resonant excitation of excitons leads to excitonic coherent polarization, which can survive up to several ps, unlike the polarization induced by excitation in the continuum which dephases on the fs time scale due to rapid free carrier scattering. The dephasing of excitonic polarization manifests as observable effects on the primary emission[4–8] in the specular reflection and transmission directions in the ps time domain. In the literature, coherence effects in excitonic reflectivity have not been studied as extensively as those in excitonic degenerate four wave mixing signals.[9] Many of the notable previous PPDR measurements[10–13] are concerned mainly with the behavior of the reflected probe pulse in the real time domain. Although a few experimental and theoretical investigations of excitonic coherence in the frequency and delay dependence of the pump-probe differential *transmission* signal are available,[14–19] very few studies of the spectrally resolved pump-probe differential *reflection* have been reported. Many aspects related to the influence on the PPDR signal of inhomogeneous broadening, many body effects such as local field, excitation induced dephasing and excitonic energy shift, and quantum interference caused by coexcitation of heavy and light hole excitons remain to be fully clarified.

In this paper, we present the results of an experimental and theoretical study of the spectrally resolved PPDR signal as a function of pump-probe delay. The experiments are performed at 8 K on 1*s* heavy and light hole excitons (*hh-x* and *lh-x*, respectively) in 17.5 nm GaAs multiple QWs (MQW) using 180 fs laser pulses. The polarization of the pump and probe pulses is either collinear ($\|$) or crosslinear ($\perp$). We find several interesting features of the delay and pump intensity dependent reflectivity spectra, to our knowledge, not reported before. To compare these results with theory, we use an expression for the PPDR signal in terms of third order excitonic polarization. In addition to a term similar to that usually used to analyze pump-probe differential transmission (PPDT) signals, the expression involves a second term which is found to be important for PPDR. We perform calculations of the PPDR signal in the frequency and delay domains in the framework of optical Bloch equations,[9] taking into account exciton inhomogeneous broadening, quantum beats due to *hh-x* and *lh-x* coexcitation, as well as many body effects such as local field (LF), excitation induced shift (EIS) in exciton energy, and excitation induced dephasing (EID). The theory can explain the coherent oscillations in PPDR spectra observed for $-ve$ delay up to several ps. The calculations show that the many body effects are essential to reproduce the experimentally observed PPDR spectral line

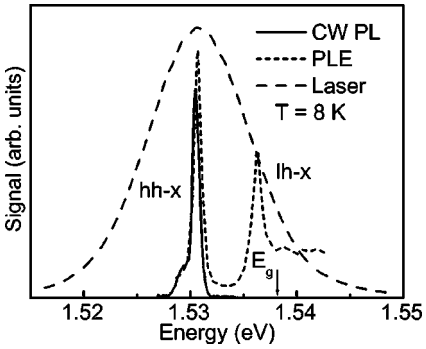

FIG. 1. CW PL and PLE spectra measured at 8 K for 17.5 nm QWs. Also shown for comparison is the energy spectrum of the probe (and pump) pulses used in the PPDR measurements.

shape at $\tau > 0$. Inhomogeneous broadening is necessary to obtain the measured spectral width. The many body effects contribute in determining the delay dependence of the signal at small $+ve$ delay. However, the signal rise at $-ve$ delays is mainly controlled by the inhomogeneous broadening. It is also sensitive to detuning of the detection energy with respect to the exciton energy. The signal decay at large $+ve$ τ is determined by the lifetime of incoherent excitons. The calculation reproduces many of the major features of quantum beats observed in the PPDR signal when coexcitation of *hh-x* and *lh-x* is included.

II. EXPERIMENTAL PROCEDURE

The molecular beam epitaxy grown MQW sample used here consists of 20 periods of 17.5 nm GaAs QWs separated by 15-nm thick $Al_{0.33}Ga_{0.67}As$ barriers. The sample is mounted in a closed cycle He refrigerator and all measurements are performed at 8 K. Continuous wave (CW) photoluminescence (PL) and PL excitation (PLE) spectra are measured using low intensity excitation by a He-Ne laser and a CW tunable Ti-sapphire laser, respectively. The PPDR measurements are performed using 180 fs pulses from a Ti-sapphire laser at a repetition rate of 82 MHz. The laser pulse spectrum shown in Fig. 1 has a full width at half maximum of about 11 meV. The pulse excitation is centered at the 1*s* *hh-x* energy. Coexcitation of *lh-x* (and a small number of free carriers) also occurs, as expected from Fig. 1. For PPDR measurements, the laser pulses are split into pump and probe parts which are cofocused (spot size $\sim 50\ \mu$m) on the sample after introducing a relative delay between them. The probe and pump beams make an angle of about 4 and 8° with the normal to the sample surface, respectively. For $\perp$ polarization case, the polarization of the probe beam is rotated by using a half wave plate. The relative angle between the probe and pump polarization was found to be 87° as given by an analyzer set for extinction (and also for maximum transmission) of the two beams. The pump beam is mechanically chopped and the probe reflection signal is detected in a lock-in amplifier. The signal is spectrally resolved using a 0.35 m monochromator before detection with a photomultiplier tube. The spectral resolution is about 0.3 meV. The average intensity (I_1) of the pump beam is typically kept one order larger than that for the probe beam (I_2), except when the dependence of the PPDR spectra on I_1 is investigated. In addition to the PPDR signal, we measure absolute reflectivity spectra for the probe pulse at increasingly high pump intensity. For this, the probe beam is chopped instead of the pump beam.

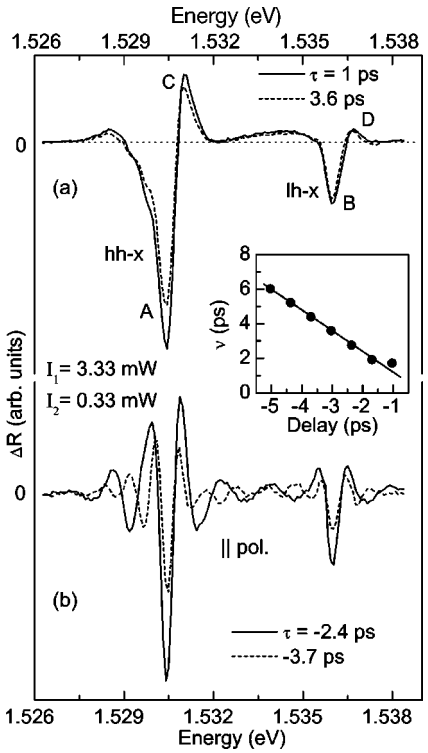

FIG. 2. Examples of PPDR spectra are shown for $\|$ polarization at $\tau = 1$ and 3.6 ps (a) and for $\tau = -2.4$ and -3.7 ps, showing spectral oscillation at $-ve$ delay (b). The oscillation frequency ν (defined as the inverse of fringe spacing in units of ps) (solid circle) as a function of delay is plotted along with a linear fit (solid line) in the inset.

III. EXPERIMENTAL RESULTS

Figure 1 shows the CW PL and the PLE spectra for the MQW sample measured at 8 K. The 1*s* *hh-x* identified at 1.5305 eV in the CW PL spectrum has a linewidth of about 0.8 meV. The small exciton linewidth and the very small Stokes shift between CW PL and PLE spectra seen in Fig. 1 indicate the high quality of the sample. The *lh-x* is identified at 1.5362 eV in the PLE spectrum. Energy of the first subband edge ($E_g \approx 1.538$ eV) is indicated in Fig. 1 with an arrow.

We have performed extensive measurements of the PPDR spectra as a function delay for both $\|$ and $\perp$ polarizations. Figure 2(a) shows, as an example, PPDR spectra obtained for $\tau = 1$ and 3.6 ps for $\|$ polarization. Here, $I_1 = 3.3$ mW and $I_2 = 0.33$ mW. The line shape mainly shows a $-ve$ peak just below the exciton energy (E_x) and a small $+ve$ peak slightly above E_x. (E_x refers to *hh-x* or *lh-x* energy, as appropriate.) This spectral line shape is different from that expected from simple Lorentz oscillator model for excitons. We

find that the line shape is essentially the same for all $\tau > 0$. The spectra for $\perp$ polarization (not shown here) have a very similar line shape, though small differences in the spectra for the two polarizations are seen on the lower energy side of the $-ve$ peaks. This is discussed later in Sec. IV.

In contrast to the case of $+ve$ delay, the spectra are strongly delay dependent for $-ve$ delay. Figure 2(b) shows two examples of the spectra measured at $-ve$ delays ($\tau = -2.4$ and -3.7 ps) in the case of $\parallel$ polarization. The following interesting features are noteworthy in Fig. 2(b). The spectral signal persists for several ps on the $-ve$ delay side (at least up to -5 ps). The delay dependence of the energy positions of the dominant $-ve$ peaks at *hh-x* and *lh-x* is negligible. The spectra show a remarkable oscillatory behavior. (The spectra for the $\perp$ case show a similar behavior. These are not shown here.) The oscillations occur not only in the energy region in which the exciton related PLE signal is seen in Fig. 1, but extend beyond that, i.e., on lower energy side of *hh-x*, at energies between *hh-x* and *lh-x* and at higher energies into the continuum states, covering a large part of the pulse spectral range. The frequency of oscillations in energy [defined as the inverse of fringe spacing in Fig. 2(b) in units of ps] increases with increasing $-ve$ τ. As the delay moves closer to zero, the oscillations begin to diminish and no oscillations are seen for $\tau \geqslant 0$. The inset in Fig. 2 shows a linear dependence of the oscillation frequency on τ for $-ve$ delays, with a slope $m \approx 1$.

The delay dependence of the absolute value of the PPDR signal at the $-ve$ peaks, marked as A and B in Fig. 2(a), is shown in Fig. 3 on semilogarithmic scale for both $\parallel$ and $\perp$ polarization with $I_1 = 3.3$ mW and $I_2 = 0.33$ mW. (The larger signal measured for $\perp$ polarization is probably a consequence of larger efficiency of the monochromator grating for $\perp$ polarization. We find that when the pump polarization is rotated instead of the probe to get the $\perp$ polarization, the signal strength is very similar for $\parallel$ and $\perp$ polarizations.) The delay dependence of the PPDR signal is similar for *hh-x* and *lh-x*. It may be noted that the signal is nonzero even when the pump pulse arrives several ps after the probe pulse ($-ve$ delay). This indicates that the polarization excited by the probe pulse survives for several ps to interfere with the delayed pump pulse. The rise of the magnitude of the PPDR signal at the $-ve$ peaks as τ (<0) approaches zero is not quite exponential. Though the delay dependence of the signal for $\tau < 0$ is very similar for $\parallel$ and $\perp$ polarizations, differences appear at small $+ve$ delay for the two polarization conditions. For the $\parallel$ polarization case, an additional, fast decaying component is seen at small $+ve$ delay. This is absent for the $\perp$ polarization case.

For a sufficiently large $+ve$ delay, beyond the coherent regime, the excitation evolves into incoherent excitons. The signal at large τ decays very slowly with τ for both polarizations, with a similar time constant of the order of a ns, determined by the lifetime of the incoherent excitons. Due to inadequate delay range (measurements were made up to about 150 ps), this may not be determined accurately in Fig. 3. A small narrow peak is visible for $\parallel$ polarization in Fig. 3 at zero delay. This is presumably the manifestation of the so

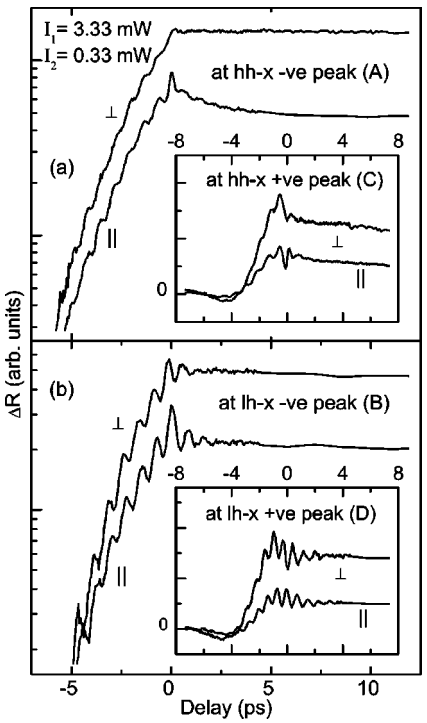

FIG. 3. Delay dependence of the absolute value of the PPDR signal at the $-ve$ peaks [marked as A and B in Fig. 2(a)] associated with *hh-x* (a) and *lh-x* (b) for $\parallel$ and $\perp$ polarization (semilogarithmic scale). Corresponding data measured at energies marked as C and D ($+ve$ peaks) in Fig. 2(a) are shown in the insets on a linear scale.

called coherent artifact for $\parallel$ polarization and is pulse width limited. This sharp peak is suppressed for $\perp$ polarization.

We may note that the PPDR signal in Fig. 3 at $-ve$ τ shows beats superposed on the approximately exponential rise for both the polarization conditions. Beats are also seen for small $+ve$ delays. The observed average beat period of 720 fs corresponds to an energy difference of 5.74 meV. This is in exact agreement with the energy separation of the *hh-x* and *lh-x* in our sample (Fig. 1). Two interesting features may be noted. First, the beats for $-ve$ delay seem to persist (undamped) as long as the signal is measurable. However, for $+ve$ delay, the beats are quickly damped. Secondly, the beats are relatively more prominent when the signal is measured at *lh-x* energy. Later, in Sec. IV, we show that both these features can be explained theoretically. In addition, we observe some phase difference in the beat oscillations between certain conditions of signal detection (at *hh-x* or *lh-x* and for excitation with $\parallel$ or $\perp$ polarizations). For example, a phase difference of nearly π is seen for signal detection at *hh-x* and *lh-x* for the $\perp$ polarization, as expected.[18] However, a somewhat smaller phase difference than expected is seen in other situations. Here, we do not investigate this aspect in detail.

In the insets of Fig. 3 is plotted (on a linear scale) the delay dependence of the signal at the $+ve$ peaks in the PPDR spectra for *hh-x* and *lh-x*, marked as C and D in Fig. 2(a), respectively. For $\tau < 0$ a marked difference can be seen between the delay dependence measured at $+ve$ and $-ve$ peaks. Although not apparent in Fig. 3 (insets) on the linear

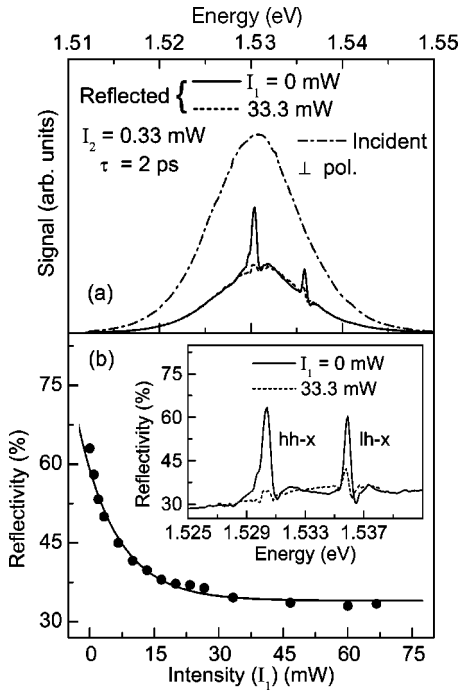

FIG. 4. (a) The incident and reflected probe spectra for zero and high (33.3 mW) pump intensity for $\tau=2$ ps and $\perp$ polarization. The absolute reflectivity spectra obtained from (a) is shown in the inset. (b) The absolute reflectivity at the *hh-x* peak is plotted as function of pump intensity (I_1).

scale used, we find that the decay is nonexponential for $\tau<0$. The delay dependence in this case shows the signal changing sign with delay. It becomes $-ve$ from $+ve$ at about $\tau=-3.5$ ps, and then again become $+ve$ at about $\tau=-6$ ps. This feature appears especially when the detuning of signal detection from E_x increases. This can be explained by the theoretical model presented in Sec. IV, as shown later. Quantum beats due to *hh-x* and *lh-x* coexcitation are clearly seen at $-ve$ delay, and even for $+ve$ delay (up to about 2 ps) for the $+ve$ peak signal. Once again, the beats are more clearly seen for measurements on *lh-x*.

It is interesting to investigate how the probe pulse reflectivity behaves as the pump pulse intensity (I_1) is increased to very large values. In Fig. 4(a), the incident and reflected probe pulse spectra are displayed for two cases: no pump and high pump intensity ($\tau=2$ ps). The *absolute* spectral reflectivity ($R=I_R/I_I$, I_I and I_R are, respectively, the incident and reflected spectral intensities) deduced from Fig. 4(a) is seen in Fig. 4(b) (inset), showing complete bleaching of the *hh-x* at high pump intensity. Saturation of the reflectivity of the probe pulse measured at the spectral peak for increasingly dense preexcitation by a pump pulse ($\tau=2$ ps) can be seen in Fig. 4(b). At saturation, the modulation of reflectivity at the *hh-x* energy by the pump pulse is about 50% (and 100% if the background is subtracted). The saturation may be caused by reduced photon to exciton conversion rate at high pump intensities due to nonlinear effects like phase space filling, stimulated population decay, etc. At only moderately large I_1, the modification of the excitonic reflectivity response for the probe pulse may be adequately treated up to

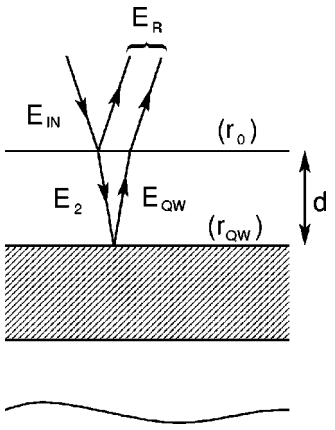

FIG. 5. The model MQW structure considered for reflectivity calculations is shown. Also, propagation directions of the incident, transmitted and reflected probe pulse electric fields are indicated schematically.

second order in pump pulse electric field. At larger I_1, higher order nonlinear terms in the pump electric field may begin to contribute. We also obtain a series of PPDR spectra for both $+ve$ and $-ve$ delay, and for both $\parallel$ and $\perp$ polarizations by varying I_1 from 1 to 67 mW, keeping the probe intensity (I_2) fixed at 0.33 mW. These spectra (not shown here) for different pump intensities have basically similar line shapes. The absolute value of the spectral signal at the main $-ve$ peaks for *hh-x* and *lh-x* obtained as a function of I_1 shows saturation beyond $I_1\approx$ 15 mW for *both* $+ve$ and $-ve$ delays. Previously, excitonic absorption saturation was studied in absorption/transmission measurements under quasicontinuous wave excitation of incoherent excitons in GaAs QWs by Masumoto *et al.*[20]

IV. DISCUSSION

In this section, we first obtain appropriate theoretical expressions for the PPDR signal. These are then evaluated within the framework of optical Bloch equations and compared with the experimental results of Sec. III.

A. Theoretical consideration

To obtain the PPDR signal, Maxwell's equations have to be solved for the propagation of the probe pulse electric field (E_2) in the sample structure including the effects of the excitonic polarization P induced in the MQWs by the probe and pump pulses. P may be obtained by solving the semiconductor Bloch equations (SBE) for the excitonic system driven by the pump and probe electric fields. We calculate the PPDR signal for near normal incidence for a model structure shown in Fig. 5. This consists of a MQW layer between a semi-infinite substrate and a cap layer of thickness d. The effects of multiple reflection within the cap layer and the MQW (ignoring the small difference in refractive index of the barrier and well regions) are neglected. Replacing the MQW region by a single effective layer of excitonic resonance for simplicity, we define the reflection coefficient of this layer to be r_{QW} and that of the cap layer r_0 (r_{QW}, r_0

<1). Retaining only linear terms in the reflection coefficients as an approximation, the reflectivity of the sample structure for an optical pulse is given as

$$R \approx |r_0 + r_{\mathrm{QW}} e^{i\phi}|^2, \tag{1}$$

where $\phi = 2dn\Omega/c$, n is the refractive index of the cap layer, c is the speed of light in vacuum, and Ω is the circular frequency of the incident light. For the conditions shown in Fig. 5, Eq. (1) can be rewritten as

$$R \propto |r_0 \mathcal{E}_2 + \mathcal{E}_{\mathrm{QW}} e^{i\phi}|^2, \tag{2}$$

where $\mathcal{E}_2$ and $\mathcal{E}_{\mathrm{QW}}$ are amplitudes of the probe electric fields incident on and reflected from the MQW layer, respectively. In absence of pump pulses $\mathcal{E}_{\mathrm{QW}} \propto i\mathcal{P}_2^{(1)}$, $\mathcal{P}_2^{(1)}$ being the linear polarization induced by the incident probe pulse. In this case, Eq. (2) takes the form

$$R \propto |\mathcal{E}_2 + iC\mathcal{P}_2^{(1)} e^{i\phi}|^2. \tag{3}$$

The constant C is determined by the relative contributions to R of the background reflectivity and the QW excitons. It may be obtained from the absolute reflectivity measurements (Fig. 4). The PPDR signal ΔR is defined as $R_{\mathrm{on}} - R_{\mathrm{off}}$ where R_{on} (R_{off}) is obtained from Eq. (2) when the QWs are excited (not excited) by the pump pulse. In calculating R_{on} we assume that the pump pulse causes modulation $\Delta\mathcal{E}_{\mathrm{QW}}$ in $\mathcal{E}_{\mathrm{QW}}$ but r_0 remains unaffected.

For a thin sample, and small depletion of incident pulse intensities, under slowly varying envelope approximation in time, the modulation $\Delta\mathcal{E}_{\mathrm{QW}}$ may be shown[21,22] to be proportional to $i\mathcal{P}^{\mathrm{NL}}$, where $\mathcal{P}^{\mathrm{NL}}$ is the amplitude of the nonlinear polarization P^{NL} induced by the pump and probe pulses, causing modulation of the probe pulse reflectivity. The lowest order term in $\mathcal{P}^{\mathrm{NL}}$ is the third order polarization $\mathcal{P}^{(3)}(t)$ which has products of the three amplitudes $\mathcal{E}_2$, $\mathcal{E}_1$, and $\mathcal{E}_1^*$ in the present case [$\mathcal{E}_1$ is the amplitude of the pump electric field (E_1)]. Note that the $\mathcal{P}^{(3)}(t)$ appearing for the PPDR signal calculation is different from that relevant for degenerate four wave mixing (DFWM) signal, which has products of the type $\mathcal{E}_2\mathcal{E}_2\mathcal{E}_1^*$ for the measurements along $2\mathbf{k}_2 - \mathbf{k}_1$ direction [$\mathbf{k}_1$ ($\mathbf{k}_2$) is the wave vector associated with E_1 (E_2)].

Taking the probe pulse to be delayed by τ from the pump pulse and keeping only the lowest order term in $\mathcal{P}^{\mathrm{NL}}$, we get the time resolved PPDR signal as

$$\Delta R(t,\tau) \propto -\mathrm{Im}[\mathcal{E}_2^*(t)\mathcal{P}^{(3)}(t,\tau)e^{i\phi}] + C\,\mathrm{Re}[\mathcal{P}_2^{*(1)}(t)\mathcal{P}^{(3)}(t,\tau)]. \tag{4}$$

Here t is the real time. Similarly, the spectrally resolved PPDR signal is given by

$$\Delta R(\omega,\tau) \propto -\mathrm{Im}[\mathcal{E}_2^*(\omega)\mathcal{P}^{(3)}(\omega,\tau)e^{i\phi}] + C\,\mathrm{Re}[\mathcal{P}_2^{*(1)}(\omega)\mathcal{P}^{(3)}(\omega,\tau)], \tag{5}$$

where $\mathcal{E}_2(\omega)$, $\mathcal{P}_2^{(1)}(\omega)$, and $\mathcal{P}^{(3)}(\omega)$ are the Fourier transforms of $\mathcal{E}_2(t)$, $\mathcal{P}_2^{(1)}(t)$, and $\mathcal{P}^{(3)}(t)$, respectively.

We emphasize that Eqs. (4) and (5) for the PPDR signal differ from the expression often used in the literature[17,23] for the pump-probe differential transmission (PPDT) signal $\{-\mathrm{Im}[\mathcal{E}_2^*(\omega)\mathcal{P}^{(3)}(\omega,\tau)]\}$. For PPDT measurements, the second term is generally much smaller than the first term and is usually not considered. But in the case of PPDR, both the terms have to be retained in general as the reflection from the surface may be comparable with that at the exciton resonance, as seen Fig. 4. [In fact, if the background reflection from the surface is made very small, as, for example, by applying antireflection coating or by performing measurements at the Brewster's angle, then the second term in Eqs. (4) and (5) will become dominant.] Therefore, in the present analysis, both the terms in Eqs. (4) and (5) have been included.

Both time and spectrally resolved PPDR signals can be obtained by calculating $\mathcal{P}_2^{(1)}(t)$ and $\mathcal{P}^{(3)}(t,\tau)$ first and then using Eqs. (4) and (5). To obtain $\mathcal{P}_2^{(1)}(t)$ and $\mathcal{P}^{(3)}(t,\tau)$, we solve the optical Bloch equations for excitons, instead of using the SBE, as a simplification. In these calculations, we include exciton inhomogeneous broadening as well as excitonic many body effects, such as the local field (LF), excitation induced shift (EIS) in exciton energy, and excitation induced dephasing (EID). Solutions to these equations for a realistic temporal profile of the subps pump and probe pulses can be obtained only by numerical computation. However, simplified expressions for $\mathcal{P}_2^{(1)}$ and $\mathcal{P}^{(3)}$ can be obtained by using the approximation of δ-like electric field pulses. Explicit expressions for $\mathcal{P}_2^{(1)}$ and $\mathcal{P}^{(3)}$ thus obtained are given in the Appendix. The essential physics can be adequately and conveniently illustrated using them. We find that the simple theory considered here is able to explain most of our PPDR measurements fairly well, without including the higher order Coulomb correlations related to biexciton transitions.

B. Simulation results and comparison with experiments

It is $\Delta R(\omega,\tau)$ that is measured in our experiments reported in Sec. III. Therefore, in what follows, we present the results of calculations[24] of $\Delta R(\omega,\tau)$, defined in Eq. (5).

Note that the parameters V and α defined in the Appendix to represent, respectively, the effects of LF and EIS enter the modified Bloch equations [Eq. (A1)] in such a way that the effect of α cannot be separated from that of V. Therefore, we indicate these as a combination (LF+EIS) in what follows and use a combined parameter [$=(V+\alpha)$] to represent them. Effect of EID is determined independently by the parameter β. In the calculation $\gamma = T_2^{-1}$ and $\Gamma = T_1^{-1}$, where T_2 and T_1 are the excitonic polarization dephasing time and exciton lifetime, respectively, and Γ_I represents exciton inhomogeneous broadening (Gaussian full width at half maximum). The parameter γ may be independently deduced from DFWM measurements. Alternatively, as shown presently, γ can be obtained from the delay dependence of the PPDR signal for $\|$ pump-probe polarization at small $+ve$ delay. Γ_I is then estimated by fitting the PL spectrum at small intensities and low temperatures. The phase factor ϕ plays an important role in determining the spectral line shape, which oscillates between absorptive and dispersive shape as ϕ changes from 0 to 2π with increase in the cap layer thickness (d). ϕ can be obtained if d is known. It can also be

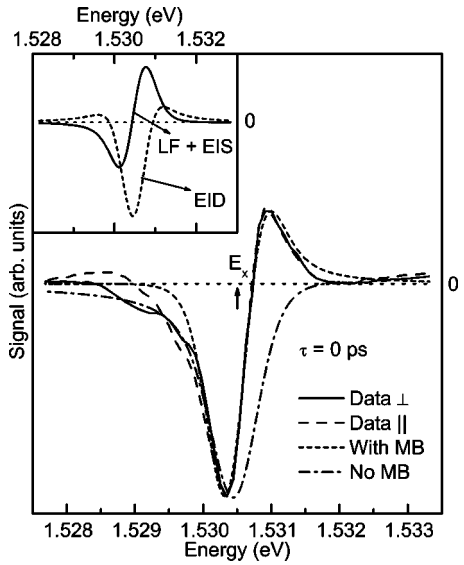

FIG. 6. Calculated PPDR spectra including inhomogeneous broadening, with and without many body (MB) effects [(LF+EIS) and EID] are compared with the measured PPDR spectra at $\tau=0$ ps for both $\|$ and $\perp$ polarization (normalized at the $-ve$ peak). Parameters used for the fit are $(V+\alpha)=2.0$ meV, $\beta=2.2$ meV, $E_x=1.5305$ eV, $\gamma=0.2$ meV, $\Gamma_I=0.6$ meV, $\Gamma=0.001$ meV. Contribution due to (LF+EIS) and EID each are separately shown in the inset.

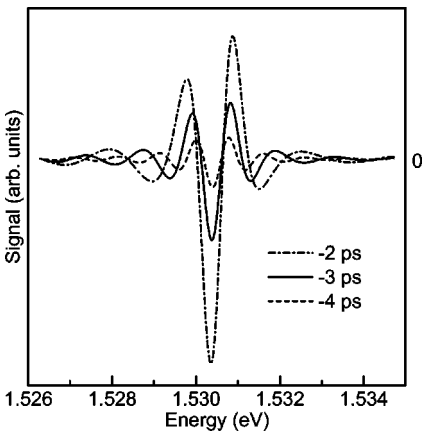

FIG. 7. Simulated PPDR spectra at $-ve$ delays ($\tau=-2$, -3, and -4 ps). These may be compared with the experimental data of Fig. 2(b). The parameters used for the calculation are the same as in Fig. 6.

deduced from the *absolute* reflectivity spectrum for the probe pulse in absence of pump excitation (Fig. 4) by using Eqs. (3) and (A11) for an inhomogeneously broadened exciton. This procedure also gives an estimate of C. With these considerations, the PPDR signals in the spectral and delay domain are simulated using $\gamma=0.2$ meV (corresponding to $T_2=3.3$ ps), $\Gamma_I=0.6$ meV, $C=0.18$, and $\phi=1.1\pi$ (modulo 2π). (d corresponding to $\phi=1.1\pi$ is about 65 nm taking $n=3.45$ for AlGaAs.) Fixing T_1 experimentally requires measurement of the PPDR signal over a much larger range of $+ve$ delay (>1 ns) than used here. However, as the calculations are rather insensitive to the choice of T_1, we set $\Gamma=0.001$ meV (corresponding to $T_1=660$ ps). E_x for *hh-x* is 1.5305 eV (Fig. 1) (E_x corresponds to $\hbar\Omega_x$ in the Appendix).

Figure 6 shows a calculation of the PPDR spectra obtained at zero delay with inhomogeneous broadening and many body effects included. Values of the parameters $(V+\alpha)(=2.0$ meV) and β $(=2.2$ meV) are so chosen as to fit the experimental PPDR spectra. [Earlier, Wang *et al.*[25] used $\beta=15\gamma$ (compared to $\beta=11\gamma$ used here) to illustrate EID effects in DFWM signal in GaAs.] Both V and α are taken to be $+ve$, indicating enhanced Lorentz local field[26] and the blueshift[27] of exciton resonance usually observed with increasing exciton density, respectively. The simulations are compared in Fig. 6 with experimental PPDR spectra measured at $\tau=0$ ps as an example for both $\|$ and $\perp$ polarizations (normalized at the $-ve$ peak). The theory is seen to explain the experimental results very well. Also shown in Fig. 6 is a calculation without including the many body effects. It is clear that a good matching of theory with experimental lineshape is not possible if the many body effects (LF+EIS) and EID are not both included. The two many body effects (LF+EIS) and EID contributing to the PPDR spectral fit in Fig. 6 are each shown separately in the inset. Among the points to be noted in Fig. 6, we may mention that the spectral data shows small features on the lower energy side of the exciton, not explained by the theory. This departure is caused by effects not included in the model. Also, a comparison of the (normalized) experimental spectra for the $\|$ and $\perp$ polarization cases shown in Fig. 6 suggests that these small effects are polarization sensitive. We find that a similar small difference occurs between PPDR spectra measured at $-ve$ delay for $\|$ and $\perp$ polarizations (not shown here). Recently, Meier *et al.*[28] showed that the difference in differential absorption spectra measured by them below the exciton resonance in InGaAs MQWs for cocircular and crosscircular pump-probe polarization is caused by dynamics of two-exciton coherent states and related fifth order nonlinear effects. Whether such effects, not included in the model used here, cause the above features in Fig. 6, or they originate due to other reasons (e.g., growth imperfection, impurity, etc.) is not clear.

Figure 7 shows calculations of the PPDR spectra at various $-ve$ delays. The oscillatory features are seen to simulate those seen in the experimental results of Fig. 2(b) very well. The frequency of spectral oscillations in the PPDR signal increases linearly with $-ve$ delay, as observed experimentally [Fig. 2 (inset)]. The calculations are performed by including the effects of (LF+EIS), EID and inhomogeneous broadening. However, we find that similar oscillatory features are obtained even when the effects of inhomogeneity, (LF+EIS) and EID are not included. The main effect of inhomogeneity in the PPDR case is to cause a reduction of the signal at the main $-ve$ peak (near E_x) with respect to other peaks whereas (LF+EIS) and EID have a compensating effect. The extent of the oscillation on the energy scale is mainly controlled by γ (Γ_I) for homogeneous (inhomogeneous) case. The origin of the oscillatory features in the PPDR spectra for $-ve$ delay is not related to the many body effects. The oscillations occur because of coherent interaction between the remnant polarization induced by the probe

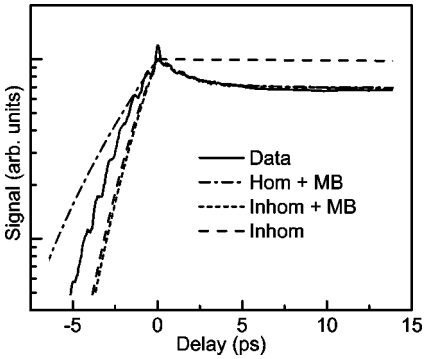

FIG. 8. Simulated delay dependence of PPDR signal at the $-ve$ peak of Fig. 6 is shown for homogeneous broadening with many body (MB) effects included, and inhomogeneous broadening with and without the MB effects. (Other parameters used for the calculation are the same as in Fig. 6.) Also, reproduced from Fig. 3(a) is the experimental delay dependence of the PPDR signal at the *hh-x* $-ve$ peak energy for $\|$ polarization.

pulse with the delayed pump pulse. This does not explicitly require any many body effects (although they do contribute to PPDR signal at $\tau<0$). This highlights an important difference between the $-ve$ delay signal for PPDR and that for DFWM. The excitonic DFWM signal observed for $\tau<0$ can be explained only by invoking Coulomb interaction induced many body effects such as LF,[29,30] EID,[25] and biexcitonic effects.[31,32] In contrast, we find here that in case of PPDR, one expects a signal at $\tau<0$ even in the absence of many body interactions [see Eq. (A4)].

Spectral oscillations near the exciton resonance, with a linear dependence of oscillation frequency on τ having a slope (m) of unity were seen earlier by Sokoloff *et al.*[15] in pump-probe *transmission* measurements on 10 nm GaAs/AlGaAs QWs (and also in bulk GaAs, CdSe, and CdS) at $-ve$ τ. Excitation and detection conditions in those experiments, however, were different from that used in our experiments. In our measurements, both pump and probe are resonant with excitons. In contrast, a broadband probe pulse is used in Ref. 15 to measure the differential *transmission* signal in the vicinity of excitons for pump excitation (i) far above the band edge (in the continuum) or (ii) well below the band edge (in the region of transparency). A theory[16,17] based on optical Bloch equations was able to reproduce the spectral oscillations. Recently, Neukirch *et al.*[19] found that while the τ dependence of the frequency of the spectral oscillations in the pump-probe differential *transmission* spectra at $\tau<0$ for excitons in ZnSe QWs corresponds to $m=1$ for energies slightly above the exciton transition, deviation from this occurs at energies below the exciton (near the exciton-biexciton transition). This was shown to be a result of four-particle (biexciton) induced correlations. In the present case, $m\approx1$ obtained in Fig. 2 (inset) was deduced from the spectral region between the *hh-x* and *lh-x* energies.

Figure 8 shows the delay dependence of the PPDR signal calculated for both homogeneously and inhomogeneously broadened cases at the energy corresponding to the $-ve$ peak of the PPDR spectrum at $\tau=0$. (The $-ve$ peak occurs at slightly different energies in the two cases.) For comparison with the calculation, experimental data corresponding to the measurement of delay dependence at the *hh-x* $-ve$ peak [marked as A in Fig. 2(a)] for $\|$ polarization, is reproduced in Fig. 8 from Fig. 3.

Consider first $\tau>0$. The theory predicts a two-exponential decay for $+ve$ delays. The fast decay near $\tau=0$ is given as $\exp(-2\gamma\tau)$. Figure 8 which displays the decay of the calculated signal with and without including the (LF+EIS) and EID clearly shows that the fast decay component is a consequence of the many body effects. Experimentally, such a two-exponential decay behavior, with a small fast decaying component near $\tau=0$ is indeed seen in the measurements of Fig. 8 in the case of $\|$ polarization. (Actually, this data is fitted to theory and the value of γ thus deduced is used in the simulations.) A double-exponential decay is, however, not evident in the measurements for the $\perp$ polarization case (Fig. 3). The origin of this difference is not known at present as we have not included the effects of pump-probe relative polarization on the PPDR signal in the theory. As expected, the decay for large $+ve$ delay is governed by the exciton lifetime irrespective of the many body effects.

As for the delay dependence for $\tau<0$ at the $-ve$ peak energy, a comparison of calculations in Fig. 8 shows that the rise of the signal with τ (<0) as τ approaches zero becomes faster in presence of inhomogeneity. In fact, the delay dependence for $\tau<0$ is mainly governed by Γ_I, the inhomogeneous linewidth, and not by γ and the many body effects, unlike the decay at small $+ve$ delay. (On the other hand, Γ_I does not affect the delay dependence of the PPDR signal for $\tau>0$.) The delay dependence of the calculated signal for $-ve$ delay is somewhat nonexponential. Figure 8 where the experimental data of Fig. 3(a) (for $\|$ polarization) is also seen, shows that the experimental curve is closely reproduced by the theoretical calculations for inhomogeneous broadening, with or without including (LF+EIS) and EID.

The above considerations are valid when the signal is measured at the $-ve$ peak energy (Fig. 6), which has only a small $-ve$ detuning from E_x. Actually, we find that the exact delay dependence of the calculated PPDR signal for $-ve$ delay is sensitive to the detuning of the detection energy E_d from E_x. This is seen in the examples of Fig. 9 where the signal is detected with different detuning Δ $(=E_d-E_x)$ within the $+ve$ and $-ve$ peaks of Fig. 6. With increasing detuning, the delay dependence shows a sign change for $-ve$ delay, the change occurring gradually closer to $\tau=0$. The signal begins to show oscillatory behavior with delay as the detuning becomes large. This feature predicted by the theory is actually seen experimentally. This is evident in the data shown in the inset of Fig. 9 where the PPDR signal is measured at the *hh-x* $+ve$ peak energy [marked as C in Fig. 2(a)] with $\Delta=0.6$ meV, at the *hh-x* $-ve$ peak [marked as A in Fig. 2(a)] with $\Delta=-0.1$ meV, and at a large $-ve$ detuning of $\Delta=-0.8$ meV.

The data in Fig. 3 shows oscillatory modulation (beats) superposed on the signal rise and decay with delay. To simulate this, the PPDR signal is calculated in the Appendix when *hh-x* and *lh-x* are coexcited. For simplicity, we do not include

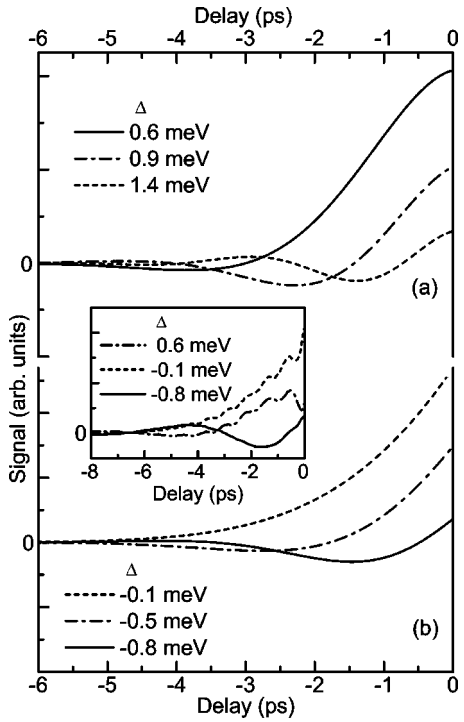

FIG. 9. Simulated delay dependence of PPDR signal for $\tau<0$ at various $+ve$ (a) and $-ve$ (b) detuning $\Delta=E_d-E_x$ (linear scale). [$+ve$ ($-ve$) Δ here corresponds to detection around the $+ve$ ($-ve$) peak of PPDR spectrum (Fig. 6). Other parameters used for the calculation are the same as in Fig. 6.] The inset shows the corresponding experimental data (linear scale).

the effects of inhomogeneity and the many body interactions. The calculation is performed following the model proposed by Schmitt-Rink *et al.*[23] However, in Ref. 23, $\mathcal{P}^{(3)}$ in the pump-probe case is obtained only for $\tau>0$. We find that $\mathcal{P}^{(3)}$ has nonzero terms for $\tau<0$, even in absence of many body effects, unlike the case of DFWM signal where inclusion of many body effects such as LF, EIS, EID, and biexcitons is essential to explain the $-ve$ τ signal.[25,29,31] The results of the simulation are shown in Fig. 10 where we plot the delay dependence of the PPDR signal at the *hh-x* and *lh-x*

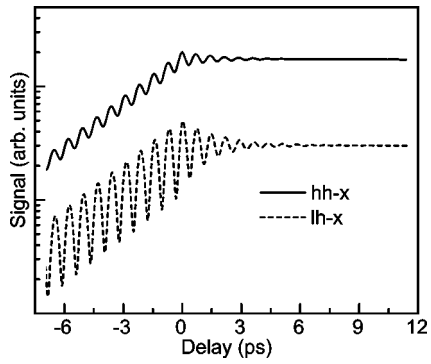

FIG. 10. Simulation of the delay dependence of the PPDR signal at the *hh-x* and *lh-x* energies showing quantum beats due to coexcitation of *hh-x* and *lh-x*. The parameters used for the calculations are $E_h=1.5305$ eV, $E_l=1.5362$ eV, $\gamma_h=\gamma_l=0.2$ meV, $\Gamma=0.001$ meV, and $\Gamma'=0.4$ meV.

energies (E_h and E_l, respectively). Quantum beats, with beat period corresponding to E_l-E_h, are readily seen in both the cases for $+ve$ and $-ve$ delays. The two main observations noted from the experimental results in Fig. 3, namely, the prominence of beats at *lh-x* energy and the quick damping of the beats for $+ve$ delays, are well reproduced in the calculation (Fig. 10). The more prominent beat at E_l is a consequence of the lower transition probability for the *lh-x* compared to that for *hh-x*. (A ratio of 1:3 is used in the calculation.[23]) Because of smaller transition probability for *lh-x*, PPDR signal is small and the effects of modulation is relatively more in this case. Also, we find that for $\tau<0$, the envelope of the beat term is governed by the difference in *hh-x* and *lh-x* dephasing time. On the other hand, for $\tau>0$, the envelope is basically governed by the dephasing rate of the coherence in heavy and light hole intervalence band transition. This being much faster compared to the exciton radiative recombination rate, a fast damping of the beats compared to the PPDR signal decay is seen on the $+ve$ delay side. The theoretical calculations do not show any phase difference in the beat oscillations for detection at *hh-x* and *lh-x*. However, as noted in Sec. III, a phase difference is seen experimentally between certain conditions of signal detection and pump-probe relative polarization. Previously, this aspect was studied in detail by Bartels *et al.*[18] who found that the phase difference was introduced by higher order Coulomb correlations including biexcitonic transitions, which are not included in our calculations.

V. SUMMARY

In summary, we have performed experimental and theoretical investigations of excitonic coherent effects in pump-probe differential reflectivity (PPDR) in GaAs QWs. The signal is nonzero even at $-ve$ delays. This arises because of nonlinear coherent interaction of the polarization left in the QWs by the probe pulse with the pump electric field. The signal rises rather nonexponentially as the delay approaches zero, with quantum beats due to coexcitation of *lh-x* and *hh-x* superposed on the rise. The delay dependence for $\tau<0$ is rather sensitive to detuning of the detection energy with respect to the exciton energy. Spectral oscillations are seen for $-ve$ delay with the oscillation frequency increasing with the $-ve$ delay. When the pump intensity becomes large, the spectra show excitonic saturation effects at both $+ve$ and $-ve$ delays. To compare the experimental results with theory, we obtain an expression for the PPDR signal in terms of the third order excitonic polarization. This has an additional term not considered earlier to describe pump-probe experiments. Using this expression, we calculate the PPDR signal in the spectral and delay domain within the framework of optical Bloch equations, incorporating quantum beats, inhomogeneous broadening, and many body effects such as local field, excitation induced energy shift and dephasing. Comparison with experiments shows that the many body effects are essential to explain the observed PPDR line shapes, and also the signal decay with τ for small $+ve$ τ but inhomogeneous broadening and detuning play a dominant role in determining the signal delay dependence for $\tau<0$.

ACKNOWLEDGMENTS

We are grateful to J. Shah and L. N. Pfeiffer for the QW sample.

APPENDIX

Here, we first present the calculation of $\mathcal{P}_2^{(1)}$ and $\mathcal{P}^{(3)}$ for a single exciton state. The effects of coexcitation of *hh-x* and *lh-x* are considered latter. In the lowest order approximation, the resonantly excited excitons may be treated as a noninteracting two-level system. The dynamics of such a system can be described by optical Bloch equations. The many body effects such as local field (LF), excitation induced shift (EIS), and excitation induced dephasing (EID) can then be introduced phenomenologically as a modification of the optical Bloch equation. We incorporate these effects for simulating the PPDR signals following the methods usually employed in the literature[25,29,33] for calculation of DFWM signals. The modified optical Bloch equations are

$$[\partial_t+\gamma'+i\omega_0']P=i[N-2\nu]|\mu|^2E'(t), \tag{A1a}$$

$$[\partial_t+\Gamma]\nu=-i[PE'^*(t)-E'(t)P^*], \tag{A1b}$$

where $E'(t)=E(t)+LP$ is the total local electric filed, E is the actual incident electric filed, $\omega_0'=\omega_0+\alpha'\nu$ represents effects of excitation induced shift of transition energy, $\gamma'=\gamma+\beta'\nu$ represents effects of excitation induced dephasing, L is the Lorentz local field factor, ν is the excited state density, P is the polarization, N is the density of the two level system, μ is the transition dipole moment, $\gamma=T_2^{-1}$ and $\Gamma=T_1^{-1}$, where T_2 and T_1, respectively, are the transverse and longitudinal relaxation times. Within rotating wave approximation, the incident electric field for the pump and probe can be written as

$$E(t)=\mathcal{E}_1(t)e^{i(\mathbf{k}_1\cdot\mathbf{r}-\Omega t)}+\mathcal{E}_2(t)e^{i(\mathbf{k}_2\cdot\mathbf{r}-\Omega t)}. \tag{A2}$$

We solve the coupled Eqs. (A1a) and (A1b) iteratively up to third order in electric filed to calculate $\mathcal{P}^{(3)}$ keeping terms containing $\mathcal{E}_2|\mathcal{E}_1|^2$ with the initial condition $P^{(0)}=0$, $\nu^{(0)}=0$. In the process, the linear polarization $\mathcal{P}_2^{(1)}$ induced by the probe pulse is also calculated. We emphasize that the $\mathcal{P}^{(3)}$ calculated here is different from that relevant for the calculation of DFWM signal.

Analytical expressions for $\mathcal{P}_2^{(1)}$ and $\mathcal{P}^{(3)}$ can be obtained in the short-pulse limit $\mathcal{E}_1(t)=\mathcal{E}_1\delta(t)$ and $\mathcal{E}_2(t)=\mathcal{E}_2\delta(t-\tau)$. These are given below for various conditions.

1. Homogeneous broadening

$$\mathcal{P}_2^{(1)}(t)\propto iN|\mu|^2\mathcal{E}_2\exp[-(\gamma+i\Omega_0)(t-\tau)]\Theta(t-\tau), \tag{A3}$$

$$\begin{aligned}\mathcal{P}^{(3)}(t,\tau)\propto -iN|\mu|^4\mathcal{E}_2|\mathcal{E}_1|^2&\exp[-(\gamma+i\Omega_0)(t-\tau)]\\&\times\left[\Theta(-\tau)\Theta(t)\left\{1+i\frac{V+\alpha-i\beta}{\Gamma}(1-e^{-\Gamma t})\right\}\right.\\&+\Theta(\tau)\Theta(t-\tau)\left\{2e^{-\Gamma\tau}+i\frac{V+\alpha-i\beta}{\Gamma}\right.\\&\left.\left.\times(2e^{-\Gamma\tau}+e^{-2\gamma\tau})(1-e^{-\Gamma(t-\tau)})\right\}\right].\end{aligned} \tag{A4}$$

Here, $\Omega_0=\omega_0-V$ is the renormalized transition energy, $V=N|\mu|^2L$, $\alpha=N\alpha'/2$, and $\beta=N\beta'/2$ are the LF, EIS, and EID parameters, respectively, and $\Theta(x)$ is the unit step function.

The above expression for $\mathcal{P}^{(3)}(t)$ obtained for the PPDR signal may be compared with that obtained by Wegener *et al.* [Eq. (13) in Ref. 29] for DFWM signal to point out the different effects of many body interactions in the two cases. Setting the many body interaction related term zero would result in a zero DFWM signal for $\tau<0$ as shown in Ref. 29. However, nonzero PPDR signal at $-ve$ τ will result due to a nonzero $\mathcal{P}^{(3)}$ even when V, α, and β are set to zero in Eq. (A4). Also, note that the $\exp(-2\gamma\tau)$ term for $\tau>0$ in Eq. (A4) occurs only when many body interactions are present. This term gives rise to the additional fast decaying component (related to excitonic polarization dephasing) at small $+ve$ delays over the exciton lifetime related slow decay for $\tau>0$. In contrast, the DFWM signal decay for $\tau>0$ is always related to exciton dephasing (and not to exciton lifetime) irrespective of whether many body effects are included or not.

We take Fourier transform of Eqs. (A3) and (A4) to get

$$\mathcal{P}_2^{(1)}(\omega)\propto iN|\mu|^2\mathcal{E}_2\frac{e^{i\omega\tau}}{\gamma+i(\Omega_0-\omega)}, \tag{A5}$$

$$\begin{aligned}\mathcal{P}^{(3)}(\omega,\tau<0)\propto -iN|\mu|^4\mathcal{E}_2|\mathcal{E}_1|^2&\exp[i\omega\tau]\exp[\gamma\tau]\\&\times\left[\frac{e^{i(\Omega_0-\omega)\tau}}{\gamma+i(\Omega_0-\omega)}+i\frac{V+\alpha-i\beta}{\Gamma}\right.\\&\left.\times\left(\frac{e^{i(\Omega_0-\omega)\tau}}{\gamma+i(\Omega_0-\omega)}-\frac{e^{i(\Omega_0-\omega)\tau}}{\Gamma+\gamma+i(\Omega_0-\omega)}\right)\right],\end{aligned} \tag{A6a}$$

$$\begin{aligned}\mathcal{P}^{(3)}(\omega,\tau>0)\propto -iN|\mu|^4\mathcal{E}_2|\mathcal{E}_1|^2&\exp[i\omega\tau]\\&\times\left[\frac{2e^{-\Gamma\tau}}{\gamma+i(\Omega_0-\omega)}+i\frac{V+\alpha-i\beta}{\Gamma}\right.\\&\times(2e^{-\Gamma\tau}+e^{-2\gamma\tau})\\&\left.\times\left(\frac{1}{\gamma+i(\Omega_0-\omega)}-\frac{1}{\Gamma+\gamma+i(\Omega_0-\omega)}\right)\right].\end{aligned} \tag{A6b}$$

2. Inhomogeneous broadening

The effect of inhomogeneous broadening can be incorporated in our model assuming a Gaussian distribution

$$g(\Omega_0)=\frac{\sqrt{4\ln 2}}{\Gamma_I\sqrt{\pi}}\exp\left[-4\ln 2\frac{(\Omega_x-\Omega_0)^2}{\Gamma_I^2}\right] \tag{A7}$$

for the transition frequencies (Ω_0). Here Ω_x is the central frequency of the inhomogeneously broadened exciton and Γ_I represents the inhomogeneous broadening. The third order polarization in that case is given by

$$\mathcal{P}^{(3)}_{\rm inh}(t,\tau)\propto\int_{-\infty}^{\infty}d\Omega_0 g(\Omega_0)\mathcal{P}^{(3)}_{\rm hom}(t,\tau,\Omega_0). \tag{A8}$$

$\mathcal{P}^{(1)}_{2\ \rm inh}(t)$ is also obtained similarly. Using $\mathcal{P}^{(1)}_{2\ \rm hom}(t,\Omega_0)$ and $\mathcal{P}^{(3)}_{\rm hom}(t,\tau,\Omega_0)$ from Eqs. (A3) and (A4) we get

$$\mathcal{P}^{(1)}_{2\ \rm inh}(t)\propto iN|\mu|^2\mathcal{E}_2\exp[-(\gamma+i\Omega_x)(t-\tau)]\times\exp\left[-\frac{\Gamma_I^2(t-\tau)^2}{16\ln 2}\right]\Theta(t-\tau), \tag{A9}$$

$$\begin{aligned}\mathcal{P}^{(3)}_{\rm inh}(t,\tau)\propto&-iN|\mu|^4\mathcal{E}_2|\mathcal{E}_1|^2\exp[-(\gamma+i\Omega_x)(t-\tau)]\times\exp\left[-\frac{\Gamma_I^2(t-\tau)^2}{16\ln 2}\right]\\&\times\left[\Theta(-\tau)\Theta(t)\left\{1+i\frac{V+\alpha-i\beta}{\Gamma}(1-e^{-\Gamma t})\right\}\right.\\&+\Theta(\tau)\Theta(t-\tau)\left\{2e^{-\Gamma\tau}+i\frac{V+\alpha-i\beta}{\Gamma}\right.\\&\left.\left.\times(2e^{-\Gamma\tau}+e^{-2\gamma\tau})(1-e^{-\Gamma(t-\tau)})\right\}\right].\end{aligned} \tag{A10}$$

Taking Fourier transform of Eqs. (A9) and (A10), we get

$$\begin{aligned}\mathcal{P}^{(1)}_{2\ \rm inh}(\omega)\propto&\,iN|\mu|^2\mathcal{E}_2\frac{\sqrt{4\pi\ln 2}}{\Gamma_I}\exp[i\omega\tau]\\&\times\exp\left(-4\ln 2\frac{(\Omega_x-\omega)^2-\gamma^2}{\Gamma_I^2}\right)\\&\times\exp\left(i8\ln 2\frac{(\Omega_x-\omega)\gamma}{\Gamma_I^2}\right)\\&\times\mathrm{erfc}\left(\frac{\sqrt{4\ln 2}}{\Gamma_I}[\gamma+i(\Omega_x-\omega)]\right),\end{aligned} \tag{A11}$$

$$\begin{aligned}&\mathcal{P}^{(3)}_{\rm inh}(\omega,\tau<0)\\&\propto-iN|\mu|^4\mathcal{E}_2|\mathcal{E}_1|^2\frac{\sqrt{4\pi\ln 2}}{\Gamma_I}\exp[i\omega\tau]\\&\times\left[\left(1+i\frac{V+\alpha-i\beta}{\Gamma}\right)\exp\left(-4\ln 2\frac{(\Omega_x-\omega)^2-\gamma^2}{\Gamma_I^2}\right)\right.\\&\times\exp\left(i8\ln 2\frac{(\Omega_x-\omega)\gamma}{\Gamma_I^2}\right)\\&\times\mathrm{erfc}\left(\frac{\sqrt{4\ln 2}}{\Gamma_I}[\gamma+i(\Omega_x-\omega)]-\frac{\tau\Gamma_I}{\sqrt{16\ln 2}}\right)\\&-i\left(\frac{V+\alpha-i\beta}{\Gamma}\right)\exp\left(-4\ln 2\frac{(\Omega_x-\omega)^2-(\Gamma+\gamma)^2}{\Gamma_I^2}\right)\\&\times\exp\left(i8\ln 2\frac{(\Omega_x-\omega)(\Gamma+\gamma)}{\Gamma_I^2}\right)\exp[-\Gamma\tau]\\&\left.\times\mathrm{erfc}\left(\frac{\sqrt{4\ln 2}}{\Gamma_I}[\Gamma+\gamma+i(\Omega_x-\omega)]-\frac{\tau\Gamma_I}{\sqrt{16\ln 2}}\right)\right],\end{aligned} \tag{A12a}$$

$$\begin{aligned}&\mathcal{P}^{(3)}_{\rm inh}(\omega,\tau>0)\\&\propto-iN|\mu|^4\mathcal{E}_2|\mathcal{E}_1|^2\frac{\sqrt{4\pi\ln 2}}{\Gamma_I}\exp[i\omega\tau]\\&\times\left\{\left[2e^{-\Gamma\tau}+i\left(\frac{V+\alpha-i\beta}{\Gamma}\right)(2e^{-\Gamma\tau}+e^{-2\gamma\tau})\right]\right.\\&\times\exp\left(-4\ln 2\frac{(\Omega_x-\omega)^2-\gamma^2}{\Gamma_I^2}\right)\exp\left(i8\ln 2\frac{(\Omega_x-\omega)\gamma}{\Gamma_I^2}\right)\\&\times\mathrm{erfc}\left(\frac{\sqrt{4\ln 2}}{\Gamma_I}[\gamma+i(\Omega_x-\omega)]\right)-i\left(\frac{V+\alpha-i\beta}{\Gamma}\right)\\&\times(2e^{-\Gamma\tau}+e^{-2\gamma\tau})\exp\left(-4\ln 2\frac{(\Omega_x-\omega)^2-(\Gamma+\gamma)^2}{\Gamma_I^2}\right)\\&\times\exp\left(i8\ln 2\frac{(\Omega_x-\omega)(\Gamma+\gamma)}{\Gamma_I^2}\right)\\&\left.\times\mathrm{erfc}\left(\frac{\sqrt{4\ln 2}}{\Gamma_I}[\Gamma+\gamma+i(\Omega_x-\omega)]\right)\right\}.\end{aligned} \tag{A12b}$$

3. Quantum beats

We now consider the effects of coexcitation of *hh-x* and *lh-x*. When *lh-x* and *hh-x* are coexcited, the exciton system can be modeled as a three-level system in which we have transitions both from heavy and light hole valence band to the common conduction band. This case was investigated by Schmitt-Rink *et al.*[23] However they had calculated only

those terms which contribute for $+ve$ delay. Here, we additionally obtain terms which contribute for $-ve$ delays. (For simplicity, here the effects of inhomogeneous broadening and many body interactions were not considered.) We solve the optical Bloch equations for three-level system[23] to get

$$\mathcal{P}_2^{(1)}(t) \propto i|\mu|^2 \mathcal{E}_2 \left[e^{-(\gamma_h + i\omega_h)(t-\tau)} + \frac{1}{3} e^{-(\gamma_l + i\omega_l)(t-\tau)} \right] \times \Theta(t-\tau), \tag{A13}$$

$$\mathcal{P}^{(3)}(t, \tau<0) \propto -i|\mu|^4 \mathcal{E}_2 |\mathcal{E}_1|^2 \Theta(t) \times \left[\frac{7}{3} e^{-(\gamma_h + i\omega_h)(t-\tau)} + \frac{5}{9} e^{-(\gamma_l + i\omega_l)(t-\tau)} + \frac{1}{3} e^{-(\gamma_h + i\omega_h)t} e^{(\gamma_l + i\omega_l)\tau} + \frac{1}{3} e^{-(\gamma_l + i\omega_l)t} e^{(\gamma_h + i\omega_h)\tau} \right], \tag{A14a}$$

$$\mathcal{P}^{(3)}(t, \tau>0) \propto -i|\mu|^4 \mathcal{E}_2 |\mathcal{E}_1|^2 \Theta(t-\tau) 2e^{-\Gamma\tau} \times \left[\frac{7}{3} e^{-(\gamma_h + i\omega_h)(t-\tau)} + \frac{5}{9} e^{-(\gamma_l + i\omega_l)(t-\tau)} + \frac{1}{3} e^{-(\Gamma' - \Gamma)\tau} \left(e^{-(\gamma_h + i\omega_h)(t-\tau)} e^{-i(\omega_h - \omega_l)\tau} + e^{-(\gamma_l + i\omega_l)(t-\tau)} e^{-i(\omega_l - \omega_h)\tau} \right) \right]. \tag{A14b}$$

Here $\gamma_{h(l)} = T_{2h(l)}^{-1}$ is the transverse dephasing rate for heavy (light) hole excitons, $\Gamma = T_1^{-1}$ is the longitudinal dephasing rate (same) for *hh-x* and *lh-x*, Γ' is the dephasing rate of coherence for heavy and light hole intervalenceband transitions, and $\omega_{h(l)}$ is the transition energy for the heavy (light) hole excitons.

We take Fourier transform of Eqs. (A13) and (A14), to get

$$\mathcal{P}_2^{(1)}(\omega) \propto i|\mu|^2 \mathcal{E}_2 e^{i\omega\tau} \left[\frac{1}{\gamma_h + i(\omega_h - \omega)} + \frac{1}{3} \frac{1}{\gamma_l + i(\omega_l - \omega)} \right], \tag{A15}$$

$$\mathcal{P}^{(3)}(\omega, \tau<0) \propto -i\mu^4 \mathcal{E}_2 |\mathcal{E}_1|^2 e^{i\omega\tau} \times \left[\frac{\frac{7}{3} e^{[\gamma_h + i(\omega_h - \omega)]\tau} + \frac{1}{3} e^{[\gamma_l + i(\omega_l - \omega)]\tau}}{\gamma_h + i(\omega_h - \omega)} + \frac{\frac{5}{9} e^{[\gamma_l + i(\omega_l - \omega)]\tau} + \frac{1}{3} e^{[\gamma_h + i(\omega_h - \omega)]\tau}}{\gamma_l + i(\omega_l - \omega)} \right], \tag{A16a}$$

$$\mathcal{P}^{(3)}(\omega, \tau>0) \propto -i\mu^4 \mathcal{E}_2 |\mathcal{E}_1|^2 e^{i\omega\tau} 2e^{-\Gamma\tau} \times \left[\frac{\frac{7}{3} + \frac{1}{3} e^{-(\Gamma' - \Gamma)\tau} e^{-i(\omega_h - \omega_l)\tau}}{\gamma_h + i(\omega_h - \omega)} + \frac{\frac{5}{9} + \frac{1}{3} e^{-(\Gamma' - \Gamma)\tau} e^{-i(\omega_l - \omega_h)\tau}}{\gamma_l + i(\omega_l - \omega)} \right]. \tag{A16b}$$

*Electronic address: bipulpal@tifr.res.in

[1] C.V. Shank, D.H. Auston, E.P. Ippen, and O. Teschke, Solid State Commun. **26**, 567 (1978); F.E. Doany and D. Grischlowsky, Appl. Phys. Lett. **52**, 36 (1987).

[2] F.E. Doany, D. Grischlowsky, and C.C. Chi, Appl. Phys. Lett. **50**, 460 (1987); S. Gupta, M.Y. Frankel, J.A. Valdamanis, J.F. Whitaker, G.A. Mourou, F.W. Smith, and A.R. Calawa, *ibid.* **59**, 3276 (1991); C. Kadow, S.B. Fleischer, J.P. Ibbetson, J.E. Bowers, A.C. Gossard, J.W. Dong, and C.J. Palmstrom, *ibid.* **75**, 3276 (1999).

[3] M.J. Lederer, V. Kolev, B. Luther-Davies, H.H. Tan, and C. Jagadish, J. Phys. D **34**, 2455 (2001).

[4] Secondary emission in nonspecular directions can also occur, either as coherent radiation in the form of resonant Rayleigh scattering (Refs. 5–7) in presence of inhomogeneities (such as QW interface roughness), or as incoherent radiation in the form of photoluminescence from incoherent excitons formed from the polarization as a result of dephasing scattering (Ref. 8).

[5] J. Hegarty, M.D. Sturge, C. Weisbuch, A.C. Gossard, and W. Wiegmann, Phys. Rev. Lett. **49**, 930 (1982).

[6] H. Stolz, *Time-Resolved Light Scattering from Excitons*, Vol. 130 of Springer Tracts in Modern Physics (Springer, Berlin, 1994).

[7] M. Gurioli, F. Bogani, A. Vinattieri, M. Colocci, Vi.I. Belitsky, A. Cantarero, and S.T. Pavlov, Solid State Commun. **97**, 389 (1996).

[8] A. Thränhardt, S. Kuckenberg, A. Knorr, T. Meier, and S.W. Koch, Phys. Rev. B **62**, 2706 (2000).

[9] See, e.g., J. Shah, *Ultrafast Spectroscopy of Semiconductors and Semiconductor Nanostructures*, 2nd ed. (Springer, Berlin, 1999).

[10] J. Aaviksoo and J. Kuhl, IEEE J. Quantum Electron. **QE-25**, 2523 (1989).

[11] D. Weber, J. Feldmann, E.O. Göbel, T. Stroucken, A. Knorr, S.W. Koch, D.S. Citrin, and K. Köhler, J. Opt. Soc. Am. B **13**, 1241 (1996).

[12] S. Haacke, R.A. Taylor, R. Zimmermann, I. Bar-Joseph, and B. Deveaud, Phys. Rev. Lett. **78**, 2228 (1997).

[13] J.J. Baumberg, A.P. Heberle, A.V. Kavokin, M.R. Vladimirova, and K. Köhler, Phys. Rev. Lett. **80**, 3567 (1998).

[14] B. Fluegel, N. Peyghambarian, G. Olbright, M. Lindberg, S.W. Koch, M. Joffre, D. Hulin, A. Migus, and A. Antonetti, Phys. Rev. Lett. **59**, 2588 (1987).

[15] J.P. Sokoloff, M. Joffre, B. Fluegel, D. Hulin, M. Lindberg, S.W. Koch, A. Migus, A. Antonetti, and N. Peyghambarian, Phys. Rev. B **38**, 7615 (1988).

[16] M. Lindberg and S.W. Koch, J. Opt. Soc. Am. B **5**, 139 (1988).

[17] M. Lindberg and S.W. Koch, Phys. Rev. B **38**, 7607 (1988).

[18] G. Bartels, G.C. Cho, T. Dekorsy, H. Kurz, A. Stahl, and K. Köhler, Phys. Rev. B **55**, 16 404 (1997).
[19] U. Neukirch, S.R. Bolton, L.J. Sham, and D.S. Chemla, Phys. Rev. B **61**, R7835 (2000).
[20] Y. Masumoto, S. Tarucha, and H. Okamoto, J. Phys. Soc. Jpn. **55**, 57 (1986).
[21] N. Bloembergen and P.S. Pershan, Phys. Rev. **128**, 606 (1962).
[22] T. Stroucken, A. Knorr, P. Thomas, and S.W. Koch, Phys. Rev. B **53**, 2026 (1996).
[23] S. Schmitt-Rink, D. Bennhardt, V. Heuckeroth, P. Thomas, P. Haring, G. Maidorn, H. Bakker, K. Leo, D.S. Kim, J. Shah, and K. Köhler, Phys. Rev. B **46**, 10 460 (1992).
[24] $\mathcal{P}^{(3)}$ calculated for $+ve$ and $-ve$ τ using the expressions in the Appendix, for δ-like electric fields in time, shows a discontinuity at $\tau=0$. While plotting, the results of calculation were normalized at $\tau=0$.
[25] H. Wang, K.B. Ferrio, D.G. Steel, P.R. Berman, Y.Z. Hu, R. Binder, and S.W. Koch, Phys. Rev. A **49**, R1551 (1994).
[26] H.A. Lorentz, *The Theory of Electrons and Its Applications to the Phenomena of Light and Radiant Heat*, 2nd ed. (Dover, New York, 1953).
[27] D. Hulin, A. Mysyrowicz, A. Antonetti, A. Migus, W.T. Masselink, H. Morkoc, H.M. Gibbs, and N. Peyghambarian, Phys. Rev. B **33**, 4389 (1986).
[28] T. Meier, S.W. Koch, P. Brick, C. Ell, G. Khitrova, and H.M. Gibbs, Phys. Rev. B **62**, 4218 (2000).
[29] M. Wegener, D.S. Chemla, S. Schmitt-Rink, and W. Schäfer, Phys. Rev. A **42**, 5675 (1990).
[30] K. Leo, M. Wegener, J. Shah, D.S. Chemla, E.O. Göbel, T.C. Damen, S. Schmitt-Rink, and W. Schäfer, Phys. Rev. Lett. **65**, 1340 (1990).
[31] K. Bott, O. Heller, D. Bennhardt, S.T. Cundiff, P. Thomas, E.J. Mayer, G.O. Smith, R. Eccleston, J. Kuhl, and K. Ploog, Phys. Rev. B **48**, 17 418 (1993).
[32] E.J. Mayer, G.O. Smith, V. Heuckeroth, J. Kuhl, K. Bott, A. Schulze, T. Meier, D. Bennhardt, S.W. Koch, P. Thomas, R. Hey, and K. Ploog, Phys. Rev. B **50**, 14 730 (1994).
[33] J.M. Shacklette and S.T. Cundiff, Phys. Rev. B **66**, 045309 (2002).